RSC Advances

PAPER

View Article Online
View Journal | View Issue

Cite this: *RSC Adv.*, 2016, **6**, 40502

Statistical experimental design, least squares-support vector machine (LS-SVM) and artificial neural network (ANN) methods for modeling the facilitated adsorption of methylene blue dye†

A. Asfaram,[a] M. Ghaedi,*[a] M. H. Ahmadi Azqhandi,[b] A. Goudarzi[c] and M. Dastkhoon[a]

This study is based on the usage of a composite of zinc sulfide nanoparticles with activated carbon (ZnS-NPs-AC) for the adsorption of methylene blue (MB) from aqueous solutions. The properties of ZnS-NPs-AC were identified by X-ray diffraction (XRD), field emission scanning electron microscopy (FE-SEM), energy dispersive X-ray spectroscopy (EDS) and Fourier transformation infrared spectroscopy (FTIR). Response surface methodology (RSM), an artificial neural network (ANN) and the least squares-support vector machine (LS-SVM) were used for the optimization and/or modeling of pH, ZnS-NPs-AC mass, MB concentration and sonication time to develop respective predictive equations for the simulation of the efficiency of MB adsorption. The obtained results using LS-SVM and ANN exhibit two nonlinear approaches (LS-SVM and ANN models) which show better performances in comparison to central composite design (CCD) for the prediction of MB adsorption. The root mean square error (RMSE) values corresponding to the validation set for MB were 0.00013, 0.00071 and 0.00117, while the respective coefficient of determination (R^2) values were 0.9996, 0.9983 and 0.9978 for the LS-SVM, ANN and CCD models, respectively. In the training set, the RMSE values of 0.00011, 0.00065 and 0.00110 and the R^2 values of 0.9997, 0.9984 and 0.9980 were obtained using the LS-SVM, ANN and multiple linear regression (MLR) models, respectively. The significant factors were optimized using CCD combined with desirability function (DF) and genetic algorithm (GA) approaches. The obtained optimum point was located in the valid region, experimental confirmation tests were conducted and good agreement was found between the predicted and experimental data. The optimum conditions for searching for the optimum point were set as pH 7.0, 0.015 g ZnS-NPs-AC, 20 mg L^{-1} MB and 3 min sonication, while at this point, the removal percentages were 98.02% and 98.12% by the DF and GA approaches, respectively. The adsorption equilibrium data in all conditions according to the optimum point are represented by the Langmuir model with a maximum monolayer adsorption capacity of 243.90 mg g^{-1} while, in all situations, the kinetics and rate of MB adsorption follow the pseudo-second-order kinetic model. Moreover, ZnS-NPs-AC was efficiently regenerated using methanol and, over five cycles, the removal percentage did not change significantly.

Received 21st January 2016
Accepted 13th April 2016

DOI: 10.1039/c6ra01874b

www.rsc.org/advances

1. Introduction

Human health and the safety and purity of environmental media depend highly on water quality which is strongly affected by the presence of contaminants, especially organic pollutants and dyes of great public concern.[1] The direct arrival of dyes contained in industrial waste water in different media causes many hazards and problems including reduced light penetration and photosynthesis efficiency, and subsequent carcinogenic and mutagenic effects. These issues encourage researchers to supply and develop new procedures to improve the quality of different ecosystems and also to increase the water quality by reducing the pollutant content to numerical values lower than threshold limits.[2,3]

Methylene blue (MB) as a heterocyclic aromatic compound has a high tendency for absorption and is easily adsorbed onto a good selection of solid materials having reasonable porosity and reactive centers.[4] MB's applicability for coloring paper, cottons and wools and also as a coating agent for paper stocks is associated with the presence of a high content of this dye that

[a]*Chemistry Department, Yasouj University, Yasouj 75918-74831, Iran. E-mail: m_ghaedi@mail.yu.ac.ir; m_ghaedi@yahoo.com; Fax: +98 741 2223048; Tel: +98 741 2223048*

[b]*Applied Chemistry Department, Faculty of Gas and Petroleum (Gachsaran), Yasouj University, Gachsaran, 75918-74831, Iran*

[c]*Department of Polymer Engineering, Golestan University, Gorgan, 49188-88369, Iran*

† Electronic supplementary information (ESI) available. See DOI: 10.1039/c6ra01874b

leads to heart damage, vomiting, shock, Heinz body formation, cyanosis, jaundice and quadriplegia, and tissue necrosis in humans.[5–7]

Adsorption, as the most conventional and high efficiency protocol, is a highly recommended versatile procedure for the removal of pollutant like dyes. This technique is based on the accumulation of molecules or ions on the surface of a solid (adsorbent).[8,9]

Adsorption processes are based on either physical or chemical forces which strongly depend on the nature of reactive centers, the charges of the adsorbent and material, the porosity of the adsorbent and also the back-bone of the adsorbent, which can target compound adsorption through several forces such as electrostatic interactions, hydrogen bonding, hydrophobic interactions, van der Waals forces *etc.*[10,11]

Activated carbon (AC), as the most conventional and popular porous structure which contains numerous functional groups, is often the best choice for water treatment purposes to achieve a safe and clean environment. However, traditional disadvantages, *viz.* high operating costs, regeneration problems and difficulties in its removal from waste water after use, limit its applications[12] and encourage researchers to find non-conventional alternative adsorbents.

Nowadays, nanomaterials because of their distinguished physical and chemical properties (high surface area, porous structure, high number of reactive atoms and large number of vacant reactive surface sites) are the best choice for loading on various supports and have led to remarkable improvements in adsorption systems. They are the most selected water treatment procedure especially in terms of economic viewpoint by enabling selection of an appropriate amount of ecofriendly material.[13–15]

The response surface methodology (RSM) technique is a good choice for estimating relationships among experimental variables and responses and representing main and interaction effects. It is possible to construct a mathematical equation that expresses the correlation between variables and responses using a small amount of reagents.[16–19]

Besides the conventional adsorption isotherms and kinetic models, statistical methods help researchers to provide more information about adsorption behaviors. Among the various multivariate statistical methods, the least squares-support vector machine (LS-SVM) and artificial neural networks (ANNs) are the best programs for modeling complex and nonlinear problems,[20,21] while multiple linear regression (MLR) efficiently explains linear relationships.[22,23]

Nowadays, a genetic algorithm (GA) approach is interesting and the most widely used variable selection method to solve the optimization problems defined by fitness criteria, applying the evolution hypothesis of Darwin and different genetic functions, *i.e.* crossover and mutation.[24,25]

In this work, a composite of zinc sulfide nanoparticles loaded on activated carbon (ZnS-NPs-AC) was synthesized, and successfully used for the removal of MB dye from contaminated water *via* an adsorption process. The major aim of this work was to evaluate the efficiencies of LS-SVM and ANN for modeling the adsorption behavior of MB onto ZnS-NPs-AC. Batch experiments were conducted in order to examine the effects of pH, adsorbent mass, initial MB concentration and sonication time on MB removal in the preliminary steps, while X-ray diffraction (XRD), field emission scanning electron microscopy (FE-SEM) and Fourier transform infrared spectroscopy (FTIR) gave detail of adsorbent structure. The isotherm and kinetic investigation provided knowledge about the mechanism of the adsorption process. Finally, the performances of the LS-SVM and ANN models were compared with those of the central composite design (CCD) models considering the correlations between the predicted and experimental data. Also, optimization results were calculated by CCD coupled with desirability function (DF) and GA methods.

2. Materials and methods

2.1. Adsorbate

MB dye (CAS number: 7220-79-3, molecular formula: $C_{16}H_{18}ClN_3S$, molecular weight: 319.85 g mol^{-1}, λ_{max}: 664 nm) was purchased from Sigma-Aldrich; its stock solutions were prepared daily by dissolution of accurately weighed amounts of dye in 100 mL water.

2.2. Instruments and reagents

Zinc sulfate dihydrate ($Zn(SO_4)\cdot 2H_2O$), tri-sodium citrate dihydrate ($Na_3C_6H_5O\cdot 2H_2O$), hexamethylenetetramine ($C_6H_{12}N_4$) and AC were purchased from Merck (Darmstadt, Germany) and thiourea (CH_3CONH_2) was purchased from Scharlau Chemie, S.A. Here, zinc sulfate and thiourea were used as the source of Zn^{2+} and S^{2-} ions, respectively, whereas hexamethylenetetramine was used as a complexing agent for Zn^{2+} ions and AC was used as a support material for the ZnS-NPs. The initial pH values of the solutions were roughly adjusted to 3.5–9.5 by adding either 0.1 mol L^{-1} HCl or NaOH. MB absorbance spectra were acquired using a UV-Vis spectrophotometer (model V-530, Jasco, Japan). The morphology of the nanoparticles was observed by FE-SEM (Hitachi S-4160, Japan) under an acceleration voltage of 15 kV. FTIR spectroscopy provided structural and compositional information on the functional groups present in the adsorbent and the approximate composition of the ZnS-NPs-AC. The spectra were recorded on a FTIR 68 (JASCO, Japan) in the range of 4000 to 400 cm^{-1} using a KBr disk containing 1% of finely ground sample. A 130 W and 40 kHz ultrasonic bath with heating system (Tecno-GAZ SPA Ultrasonic System, Bologna, Italy) was used for the ultrasound-assisted adsorption. XRD (Philips PW 1800, The Netherlands) was performed to characterize the phase and structure of the prepared nanoparticles using $Cu_{K\alpha}$ radiation (40 kV and 40 mA) at angles ranging from 20 to 70°. The point of zero charge (pH_{zpc}) was determined for the ZnS-NPs-AC as follows: a 10 mL solution of KNO_3 (0.1 mol L^{-1}) was added to 0.1 g of adsorbent. The initial pH values were adjusted in the range 1.0–10.0 by adding HCl and/or NaOH solutions, and the solutions were then stirred for 24 h at 25 °C. After filtering the mixtures, the differences between the final and initial pH values (ΔpH) of the solutions were plotted against initial pH.

2.3. Preparation of ZnS nanoparticles loaded on activated carbon

ZnS-NPs-AC was prepared according to the recommended procedure: 50 mL of 0.01 mol $Zn(SO_4)\cdot 2H_2O$ solution and 0.005 mol $Na_3C_6H_5O\cdot 2H_2O$ solution were mixed completely and diluted to a total volume of 200 mL. In the next step, 100 mL of 0.2 mol L^{-1} CH_3CONH_2 solution was added to the prepared mixed solution drop-by-drop along with strong stirring at room temperature over 45 min in an Erlenmeyer flask. The obtained mixed solution was stirred at room temperature for 15 h, then stirred at 95 °C for 1.5 h. Finally, the material produced was deposited on 20 g AC following stirring for 3 h.

2.4. Batch adsorption experiments

To conduct batch adsorption experiments, 50 mL of 20 mg L^{-1} MB at pH 7.0 was mixed completely with 0.015 g ZnS-NPs-AC following sonication for 3 min, and subsequently around 10 mL of the supernatant solution was centrifuged for 3 min at 3500 rpm. The concentration of dye in the supernatant solution before and after adsorption was determined by UV-Vis spectrophotometry at λ_{max} of 664 nm. The MB removal percentage was calculated by:

$$R\%\ \mathrm{MB} = \left(\frac{A_0 - A}{A_0}\right) \times 100\% \quad (1)$$

where A_0 is the initial absorbance and A is the equilibrium absorbance at the MB maximum absorption wavelength. The adsorption capacity for MB at time t (q_t; mg g^{-1}) was calculated using the following equation:

$$q_t = \left(\frac{(C_0 - C_t)V}{W}\right) \quad (2)$$

where C_t (mg L^{-1}) is the MB concentration at time t (min), C_0 is the initial concentration (mg L^{-1}), W is the adsorbent mass (g), and V is the solution volume (L).

Kinetic studies were undertaken at various MB concentrations (8–40 mg L^{-1}). MB was mixed sonically with 0.015 g ZnS-NPs-AC at 25 °C at pH 7.0 over time intervals of 0.5–6 min, while after each time point, phase separation was accomplished by centrifugation and the supernatant was analyzed by spectrophotometry.

Isotherm studies were conducted over the MB concentration range of 5–40 mg L^{-1} using 0.005–0.025 g ZnS-NPs-AC at 25 °C and pH 7.0 following 3 min sonication. After equilibrium, the MB concentration was determined according to a calibration curve obtained at the same conditions.

2.5. Multivariate experimental design and optimization

RSM following CCD analysis indicates the numerical values for significant terms in the obtained polynomial equation for the main and interaction effects. This enables the researchers to predict adsorption data over expected space.[26] The influence of four main parameters, namely pH (X_1; 3.5–9.5), adsorbent mass (X_2; 0.005–0.025 g), initial MB concentration (X_3; 8–40 mg L^{-1}) and sonication time (X_4; 1–5), on MB removal was investigated with CCD using the minimum number of experiments.

The ranges and the levels of the variables are shown in Table 1 for 30 experiments composed of 16, 8 and 6 for factorial, axial and replicates at the center points, respectively. The second-order polynomial response equation correlates the dependency of a response to a significant term which may be either a main or an interaction effect[27] as presented according to previous reports.[28–30]

The quality of prediction and fitting of the polynomial model was expressed through the coefficient of determination R^2 and Adj-R^2.[17]

To compare the range of the predicted values at the design points to the average prediction error, the metric "adequate precision (AP)" was used according to the following formula:[31]

$$\mathrm{AP} = \frac{\max\ (\bar{y}) - \min\ (\bar{y})}{\sqrt{\overline{V}(\bar{y})}} \quad (3)$$

$$\sqrt{\overline{V}(\bar{y})} = \frac{1}{n}\sum_{i=1}^{n}\overline{V}(\bar{y}) = \frac{\rho\sigma^2}{2} \quad (4)$$

where y, ρ and σ demonstrate the predicted value, the number of model parameters and the residual mean square from the analysis of variance (ANOVA) table, respectively, and n represents the number of experiments. According to the coefficients of each term in the empirical model, judgments about the significant contribution of each term based on the P-value, and the fitted polynomial equation were undertaken in the form of contour and surface plots. Finally, additional confirmation experiments were carried out to verify the accuracy of the statistical experimental design. All the experimental design and data analysis was performed using STATISTICA software package version 10.0.

2.6. LS-SVM dye removal modeling

SVM as a learning method was developed by Vapnik[32] and is a powerful tool. This supervised learning method can be used for regression or classification in nonlinear models, and density estimation leads to complex optimization problems, typically quadratic programming.[33] However, this method (SVM) is often time consuming and difficult to adapt, suffering from the problem of a large memory requirement and CPU time when trained in batch mode. This limitation is overcome by LS-SVM as the modified version of SVM which solves the set of linear equations instead of the quadratic programming problem to minimize the complex nature of the optimization processes.[34] The theory and more details of SVM and LS-SVM can be found in the literature.[35] The LS-SVM equation can be expressed as follows:

$$y(x) = \sum_{i=1}^{N}(\alpha - \alpha^*)K(X, X_i) + b, \quad 0 \le \alpha_i, \alpha^* \le \gamma \quad (5)$$

where b is bias value, α_i and $\alpha^*$are the Lagrange multipliers, K(X, X_i) is the kernel function, and γ is the regularization parameter, determining the trade-off between the fitting error minimization and the smoothness of the estimated function. Many kernel functions have been presented in the literature, such as the linear kernel, radial basis function (RBF), sigmoid kernel and polynomial kernel. The selection of the proper

Table 1 Coded, actual levels and the experimentally observed and predicted responses used in the experimental design[a]

		Levels				
Factors	Unit	$-\alpha$	Low (−1)	Central (0)	High (+1)	$+\alpha$
X_1: pH	—	3.5	5.0	6.5	8.0	9.5
X_2: adsorbent mass	g	0.005	0.010	0.015	0.020	0.025
X_3: MB concentration	(mg L^{-1})	8	16	24	32	40
X_4: sonication time	min	1	2	3	4	5

	Factors				R% MB		
Run	X_1	X_2	X_3	X_4	Observed[b]	Predicted[c]	Residual[d]
1	5.0	0.010	16	2	85.5900	85.6106	−0.0206
2	8.0	0.010	16	2	94.0100	94.0474	−0.0374
3	5.0	0.020	16	2	95.4340	95.1541	0.2799
4	8.0	0.020	16	2	98.1200	98.4457	−0.3257
5	5.0	0.010	32	2	80.4500	80.5179	−0.0679
6	8.0	0.010	32	2	88.2000	87.9416	0.2584
7	5.0	0.020	32	2	91.0220	91.1347	−0.1127
8	8.0	0.020	32	2	93.3100	93.4131	−0.1031
9	5.0	0.010	16	4	87.2400	87.0254	0.2146
10	8.0	0.010	16	4	90.5610	90.6206	−0.0596
11	5.0	0.020	16	4	98.5000	98.9307	−0.4307
12	8.0	0.020	16	4	97.5600	97.3806	0.1794
13	5.0	0.010	32	4	86.2400	86.0866	0.1534
14	8.0	0.010	32	4	88.5000	88.6684	−0.1684
15	5.0	0.020	32	4	99.2140	99.0651	0.1489
16	8.0	0.020	32	4	96.3500	96.5017	−0.1517
17	3.5	0.015	24	3	85.8500	85.9629	−0.1129
18	9.5	0.015	24	3	92.0100	91.8364	0.1736
19	6.5	0.005	24	3	78.2592	78.4258	−0.1666
20	6.5	0.025	24	3	96.0300	95.8026	0.2274
21	6.5	0.015	8	3	98.3600	98.2904	0.0696
22	6.5	0.015	40	3	92.3100	92.3189	−0.0089
23	6.5	0.015	24	1	94.1000	94.0659	0.0341
24	6.5	0.015	24	5	98.5960	98.5694	0.0266
25 (C)	6.5	0.015	24	3	97.8740	97.2618	0.6122
26 (C)	6.5	0.015	24	3	96.5100	97.2618	−0.7518
27 (C)	6.5	0.015	24	3	97.4470	97.2618	0.1852
28 (C)	6.5	0.015	24	3	96.8000	97.2618	−0.4618
29 (C)	6.5	0.015	24	3	97.7600	97.2618	0.4982
30 (C)	6.5	0.015	24	3	97.1800	97.2618	−0.0818

[a] (C): center point. [b] Experimental values of response. [c] Predicted values of response by the proposed RSM model. [d] Difference between the actual and predicted values for each point in the design.

kernel function to map the nonlinear input space into a linear feature space depends on the distribution of the training data in the feature space.[36] The function RBF is broadly employed in regression problems, because RBF can be substantially faster to train than other kernel functions. The RBF can be expressed as:

$$k(\bar{x}_i,\bar{x}_j) = \exp(-\gamma\|\bar{x}_i - \bar{x}_j\|^2) \quad (6)$$

2.7. Principle of ANN model

ANN is an information processing system made up of signal processing elements called neurons. ANN cannot create an equation similar to RSM; it behaves like a human brain and estimates the response based on the trained data in the range in question.

In general, ANN is a parallel dynamic system of highly interconnected structures consisting of an input layer of neurons (input variables), a number of hidden layers, and an output layer (response or responses). The strengths of the connections between inputs, hidden layers and output layers are determined by weights (w) and biases (b) that are known as the parameters of the ANN.

The main step in the development of an ANN model is the optimization of the ANN topology for the study.[37] In this work, the influence of inputs (*viz.* pH, initial MB concentration, adsorbent mass and sonication time) on the output, MB removal efficiency (R (%)), was optimized and studied. It should be noted that the experimental results (30 data sets; Table 1) were used for ANN modeling. It is known that the choice of the number of neurons in the hidden layer can have a considerable impact on the

performance of the network. In order to determine the optimum number of hidden nodes, a series of topologies were used, in which the number of nodes was varied from 2 to 15.

The Levenberg–Marquardt (LMA) algorithm is a standard technique and more successive in its prediction of performance for complex relationships between input variables. It is used to solve nonlinear least squares problems. This is one of the most popular methods used in neural network applications because of its relatively high speed, and because it is highly recommended as a first choice supervised algorithm, although it does require more memory than other algorithms.

A sigmoid function is the most widely used transfer function for the hidden and output layers in back propagation (BP) networks, because it is differentiable. Therefore, the sigmoid transfer function was applied for the hidden and output layers.

The theory and more details of LMA and ANN can be found in the literature.[38] The best topologies were selected from the maximum R^2 values and minimum mean squared error (MSE) values.

In the present study, all experimental results were normalized within a uniform range of −1 and +1 according to the equation below:[39]

$$z_i = 0.8 \times \left(\frac{x_i - x_{\min}}{x_{\max} - x_{\min}} \right) + 0.1 \quad (7)$$

where z_i is the normalized value of x_i. The $x_{\max}$ and $x_{\min}$ are the maximum and minimum value of x_i, respectively. The data were randomly divided into two groups (75% training and 25% testing).

2.8. Principle of GA

GA is defined as a random global search technique, used in computing to find out an exact or estimated solution in order to optimize and investigate a problem.[40] Solutions from one population are used to form a new population that must be better than the old one. The above process is repeated until the best fit is found, while the GA explores all regions of the solution space using individual populations which represent a set of independent variables.[40]

3. Results and discussion

3.1. Characterization of ZnS-NPs-AC

FE-SEM of ZnS-NPs-AC (Fig. 1a and b) reveals its amorphous morphology and/or the spherical shape with sizes in the range of 50–100 nm.

The XRD pattern of the ZnO nanospheres (Fig. 1c) consists of (111), (220) and (311) peaks corresponding to the zinc blende structure (cubic, b-ZnS; JCPDS no. 05-0566). The peak broadening in the XRD pattern clearly indicates the presence of nanocrystals of ZnS with very small size, while the average size based on the Debye–Scherrer formula ($D = 0.89\lambda/\beta \cos\theta$) using the (111) diffraction peak is around 40 nm.

Energy dispersive X-ray spectroscopy (EDS) of the ZnS-NPs-AC (Fig. 1d) based on the localized elemental information shows the presence of C, Zn and S as the dominant elements throughout the surface of the adsorbent, with weight percentages of 95.30, 2.60 and 2.10%, respectively.

The FTIR spectrum of the ZnS nanoparticles (Fig. 2a) is composed of peaks around 1128.5, 998.08, and 624.60 cm^{-1}

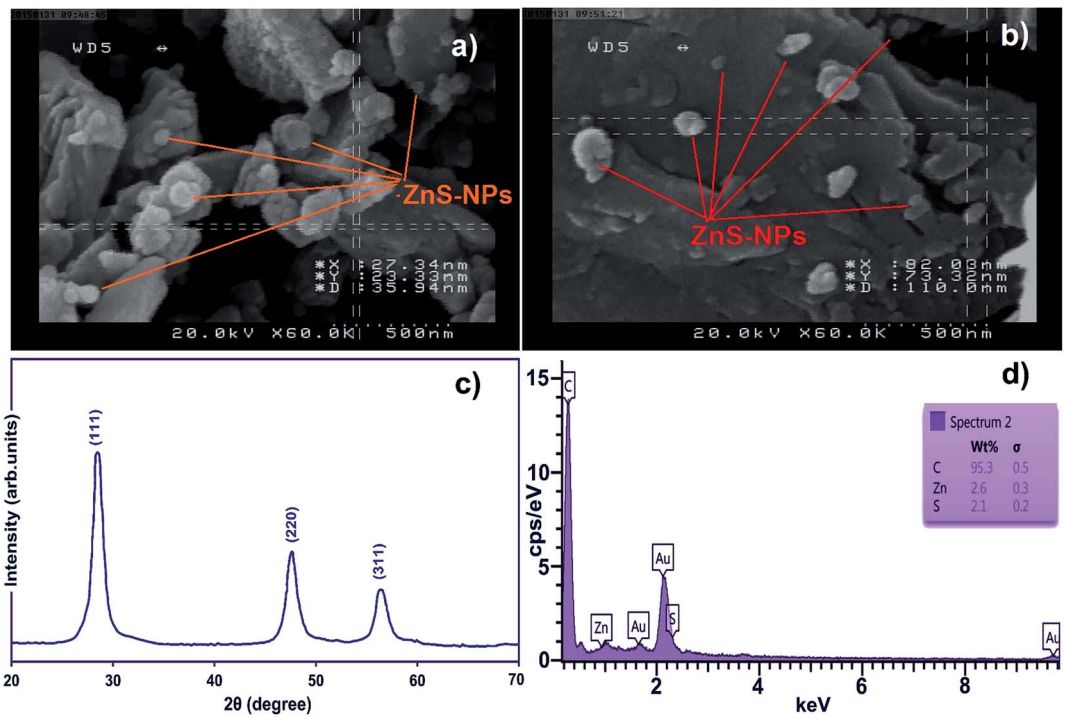

Fig. 1 (a and b) FE-SEM images, (c) XRD pattern and (d) EDS of ZnS-NP-AC.

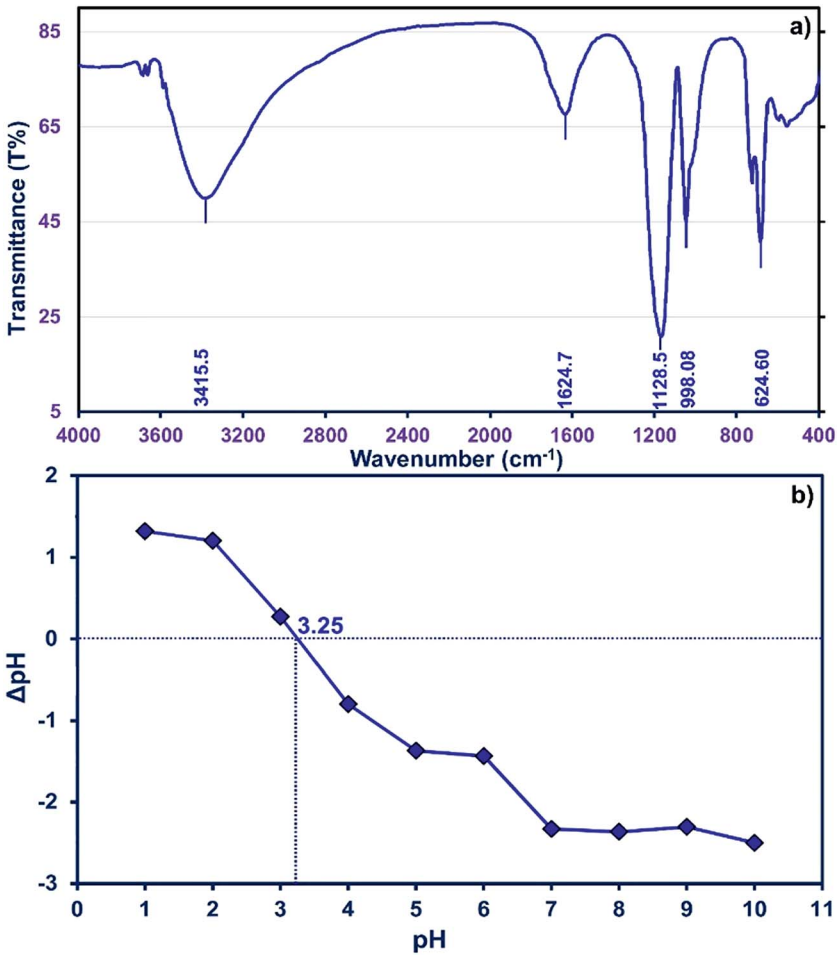

Fig. 2 (a) FTIR spectrum and (b) pH_{zpc} obtained from ZnS-NP-AC.

showing good agreement with previously reported results.[41,42] The observed peak at 1624.7 cm^{-1} is assigned to the C=O stretching mode, while broad absorption peaks in the 3100–3600 cm^{-1} interval correspond to O–H stretching modes arising from the absorption of water on the surface of the nanoparticles *via* –COOH groups or even the AC functional groups.

The neutral charge of the adsorbent surface at pH_{ZPC} becomes negative at pH values higher and positive at pH values lower than this value, respectively.[43] Data of ΔpH ($pH_{final} - pH_{initial}$) *vs.* pH were plotted (Fig. 2b) and reveal that pH_{zpc} is 3.25 for ZnS-NPs-AC. Therefore, at pH values greater than 3.25 the removal should be higher due to increased electrostatic interactions. Generally, the net positive charge of adsorbate decreases at higher pH and is associated with a decrease in the repulsion between the adsorbent surface and the cationic MB dye.

3.2. CCD model and statistical analysis

RSM is an efficient technique for optimization and was applied to analyze the effect of the important parameters and their interactions on the adsorption process under different conditions using CCD.[15]

The factors affecting MB removal efficiency should be more keenly monitored so that better systems can be developed to remove dyes from waste waters on a pilot scale. Hence, in this study, the CCD was applied to optimize the adsorption of MB dye from dye solution by varying the parameters pH, adsorbent mass, MB concentration and contact time in the preliminary steps, while the numerical values of various runs and respective experimental responses are detailed in Table 1.

The analysis of CCD results led to the following second-order polynomial equation:

$$\begin{aligned} Y_{R\%\ \mathrm{MB}} = {} & -8.3 + 18.6X_1 + 4512.7X_2 - 0.2X_3 + 2.9X_4 \\ & - 171.5X_1X_2 - 0.02X_1X_3 - 0.81X_1X_4 + 6.71X_2X_3 \\ & + 118.1X_2X_4 + 0.13X_3X_4 - 0.93{X_1}^2 - 101\,476.22{X_2}^2 \\ & - 0.01{X_3}^2 - 0.24{X_4}^2 \end{aligned} \quad (8)$$

ANOVA based on *F*- and *P*-tests gives information about the type of contribution of each term to the response and quality of the regression equation (Table 2).

The statistical significance of the model is assigned according to the *F*-value. The "Model *F*-value" of 448.035 is a good indication of the high efficiency and applicability of the present model and denotes that there is only 0.01% chance of obtaining

Table 2 ANOVA, regression coefficients and quadratic summary statistics for CCD (MB)

Source of variation	Sum of square	Degree of freedom	Mean square	*F*-value	*P*-value	Status	Regression coefficients: Factor	Regression coefficients: Coefficient estimate
Model	927.0695	14	66.2192	448.0346	<0.0001	Significant	Intercept	−8.325
X_1-pH	51.7470	1	51.7470	350.1165	<0.0001		X_1	+18.560
X_2-adsorbent mass	452.9279	1	452.9279	3064.4772	<0.0001		X_2	+4513.0
X_3-MB concentration	53.4882	1	53.4882	361.8974	<0.0001		X_3	−0.172
X_4-sonication time	30.4223	1	30.4223	205.8349	<0.0001		X_4	+2.901
X_1X_2	26.4736	1	26.4736	179.1184	<0.0001		X_1X_2	−171.5
X_1X_3	1.0267	1	1.0267	6.9464	0.01872		X_1X_3	−0.021
X_1X_4	23.4425	1	23.4425	158.6105	<0.0001		X_1X_4	−0.807
X_2X_3	1.1519	1	1.1519	7.7934	0.01369		X_2X_3	+6.708
X_2X_4	5.5779	1	5.5779	37.7394	<0.0001		X_2X_4	+118.10
X_3X_4	17.2536	1	17.2536	116.7369	<0.0001		X_3X_4	+0.130
X_1^2	119.8745	1	119.8745	811.0625	<0.0001		X_1^2	−0.929
X_2^2	176.5272	1	176.5272	1194.3705	<0.0001		X_2^2	−101 500.0
X_3^2	6.5670	1	6.5670	44.4316	<0.0001		X_3^2	−0.008
X_4^2	1.5284	1	1.5284	10.3410	0.005775		X_4^2	−0.236
Residual	2.2170	15	0.1478					
Lack of fit	0.7745	10	0.0775	0.2685	0.9635	Not significant		
Pure error	1.4424	5	0.2885					
Cor total	929.2865	29						

Quadratic summary statistics	R^2	Adj-R^2	Pred-R^2	Std dev.	CV%	PRESS	Adequate precision
Response (R% MB)	0.9976	0.9954	0.9930	0.3844	0.4135	6.539	75.92

this value due to noise. A very low probability value (*P*-value < 0.0001) implies that the model is strongly significant at a 95% confidence interval (*i.e.*, *P*-values less than 0.05 indicate significance). The non-significant lack-of-fit is favorable and specifies the high predictability of the model. The "Lack of Fit *F*-value" (0.2685) strongly indicates its low contribution compared to pure error. In Table 2, the *P*-values < 0.050 are significant.

The R^2 value of 0.9976 indicates that 99.76% of the variability can be explained in random fashion changes in the variable. The R^2-predicted value of 0.9930 is in reasonable agreement with the R^2-adjusted value of 0.9954. Fig. 3a indicates that the predicted values of MB adsorption efficiency obtained from the model and the actual experimental data are in good agreement which is evidence for the validity of the regression model. Fig. 3b shows the residual plot *versus* predicted data and the random pattern of residuals exhibits the model's adequacy.

An adequate precision (signal-to-noise ratio) value higher than 4 supports the desirability of the model; a value of 75.92 was found in the present study. Hence this model can navigate the design space.[44] The degree of precision and reliability given by the coefficient of variation (CV) (0.4135%) shows the higher precision and reliability of experimental data.[45]

The normal distribution of data was traced by plotting the residuals and deviations of the observed data values from the predicted values (Fig. 3c). A visual examination of the data shows that the data points fall approximately along a straight line for MB adsorption and also suggests the fair adequacy of the constructed equation for predicting the adsorption and estimating individual interactions between the response and process parameters.

3.3. Model graphs for the effect of variables

The results from a plot of perturbation response (R% MB) against the factors (Fig. 4a) show evidence for the importance of pH (X_1), adsorbent mass (X_2), MB concentration (X_3) and sonication time (X_4) in the MB removal process. Fig. 4 shows the MB removal percentage in terms of raising each variable in turn while all other factors are held in the middle of the design space (the coded zero level). The influence of the adsorbent mass on the removal percentage became more pronounced when moving from the middle towards the higher levels. The reciprocal slope of the perturbation curve for factor X_2 (MB concentration) is related to a decrease in MB removal when increasing the MB concentration up to 40 mg L^{-1}. The reciprocal slope of the perturbation curve for X_1 and X_4 (pH and sonication time) confirmed that maximum MB removal is seen at pH 7.0 and 5 min.

The main effects of each parameter on the MB removal efficiency (Fig. 4) show that both pH and adsorbent mass have a positive correlation with the removal percentage (Fig. 4b) that is attributed to the increase in availability of binding sites at a higher initial solution pH and the enhancement of the accessibility of dye for binding sites of adsorbent.[43] The problem with high adsorbent mass however is that it may cause interference between binding sites or there may be insufficient dye ions in the solution with respect to the available binding

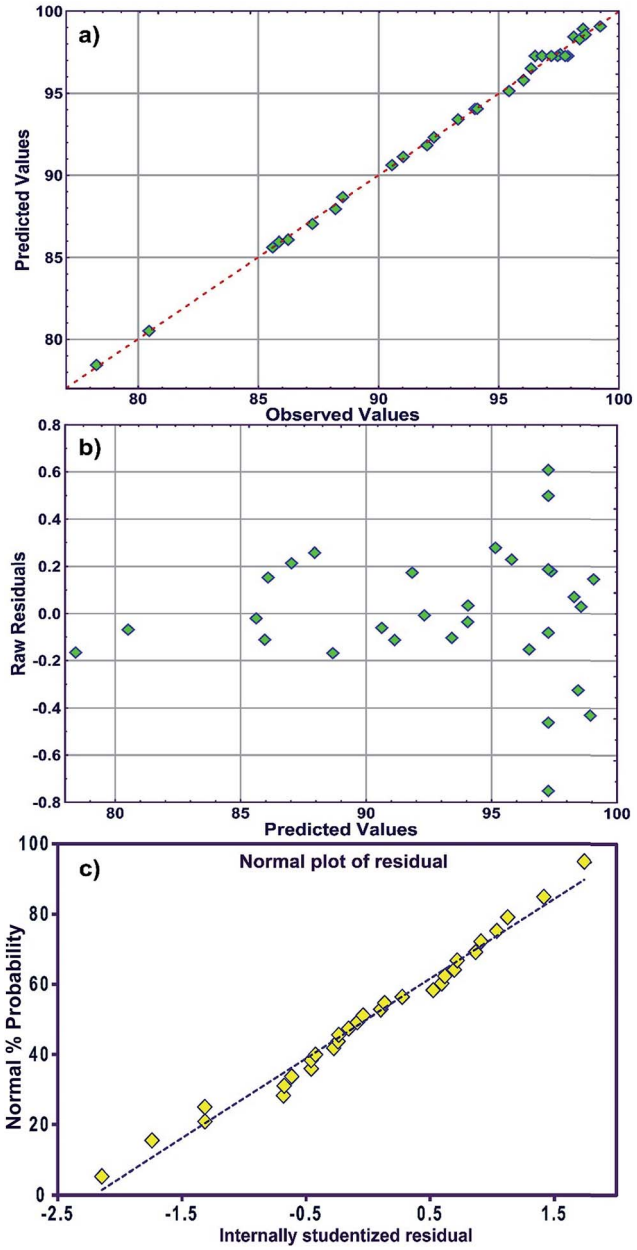

Fig. 3 (a) Plot of the measured and model-predicted values of the response variable, (b) residuals *versus* predicted removal percentage (*R*%) and (c) the normal probability plot of the residuals.

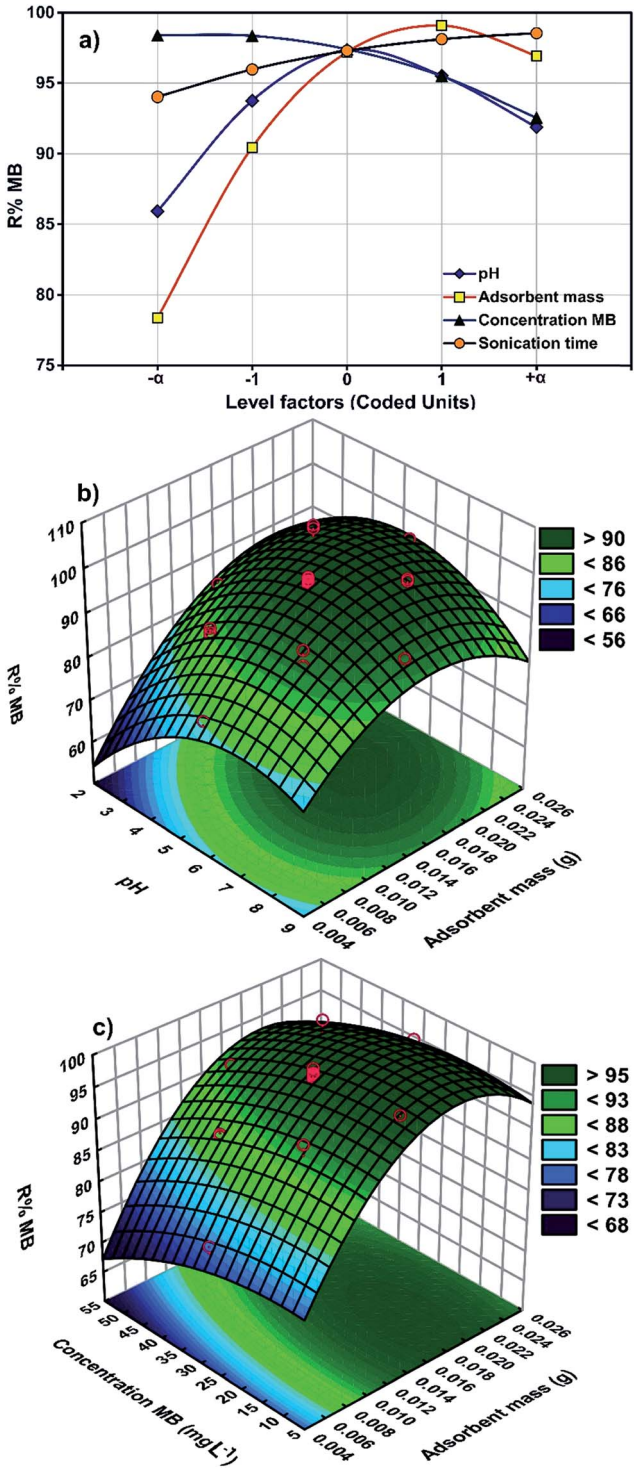

Fig. 4 (a) Overlay plot of the perturbation of all the variables on dye removal. Response surface plot and contour graph to illustrate the effects of (b) pH and adsorbent mass and (c) adsorbent mass and concentration of MB on MB removal using ZnS-NP-AC.

sites. It is likely that protons will then combine with dye ions and thereby decrease the interaction of dye ions with the ZnS-NP-AC components.

The pH_{zpc} of ZnS-NP-AC was equal to 3.25 (Fig. 2b) and therefore, basic solution favors MB adsorption onto the ZnS-NP-AC. This is favorable for the studied adsorption system for real waste water decolorization from the textile industry (alkaline) because it avoids additional costs for pH control.

The combined effects of adsorbent mass and MB concentration (Fig. 4c) reveal the reverse impact of MB concentration and adsorbent mass on MB uptake. At lower adsorbent mass, an increase in MB concentration led to saturation of the binding sites and finally a decline in uptake. A higher adsorbent mass enhanced the uptake which may be related to the availability of relatively more active binding sites.

3.4. Analysis of AAN

In this research, ANN models have been used to evaluate the effect of four input variables, namely pH, adsorbent mass, MB concentration and sonication time, on the removal percentage of MB as the output. A feed-forward topology of the ANN model, famous as a multilayer perceptron (MLP), has been used with a BP algorithm to build the predictive models.

The optimization of the network is a very important step in network training that is based on the optimization of a number of neurons in the hidden layer. For this purpose, different numbers of neurons (2–15 neurons corresponding to the hidden layer) were tested and it was found that a hidden layer with 8 neuron was the best case and permitted achievement of good operation parameters with a minimum value of MSE and a maximum value of R^2. As a result, in this study a three layered feed-forward BP ANN (4 : 8 : 1) was used for modeling of the adsorption process. Fig. 5a displays the goodness of fit between the forecast values for the removal of data using the ANN model against the actual values for the CCD matrix.

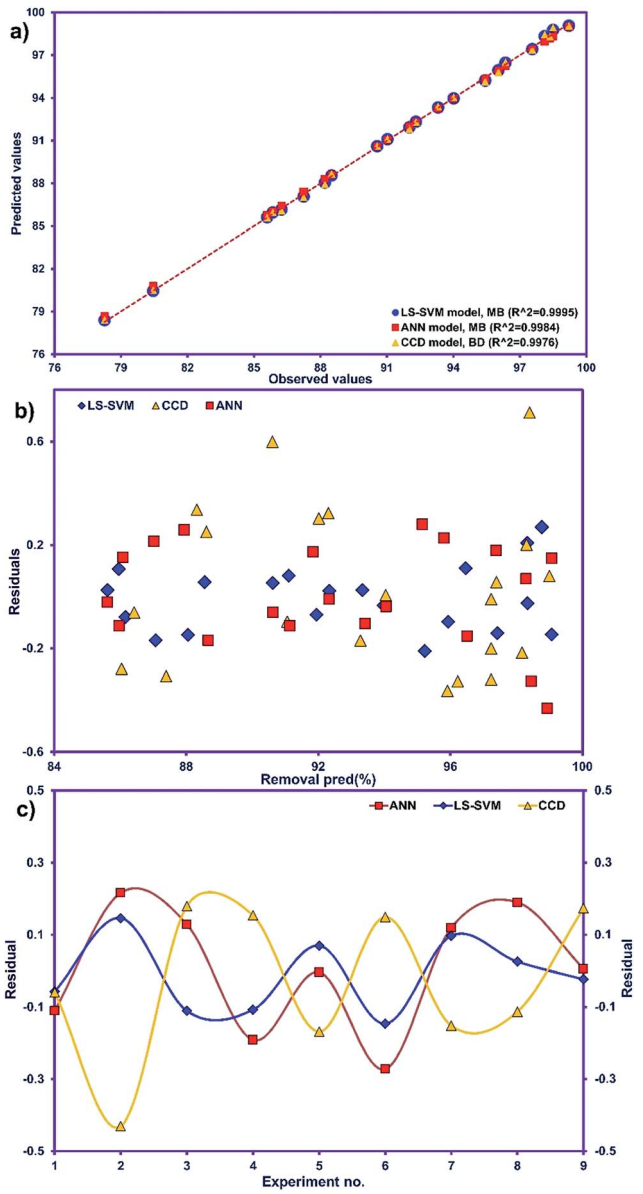

Fig. 5 (a) Scatter plot of predicted values from the RSM, ANN and LS-SVM models *versus* actual values for the CCD matrix, (b) plot of the residuals *versus* model-predicted values and (c) distribution of residuals for the LS-SVM, ANN and RSM models.

3.5. Analysis of LS-SVM

The constructed LS-SVM model with the RBF kernel function was applied to the selected data set to predict MB adsorption using the set of four variables as estimators. A two-step grid search method with a tenfold cross-validation was used to derive the LS-SVM model parameters. The optimal values for the LS-SVM model parameters, C (cost constant), ε (the radius of the insensitive tube) and kernel-dependent parameter (γ) were found to be 672.34, 0.002, and 1.327, respectively, and the number of SVs was 185; the statistical parameter values are summarized in Table 3. It may be noted that the model-predicted values of the dependent variable have a high correlation with the experimental values in all three sets (R^2 was 0.9997 in training and 0.9996 for the validation data). Values of other criteria parameters suggest a good fit of the LS-SVM model to the datasets and the adequacy of the selected model for predicting the adsorptive removal of MB.

3.6. Comparison of RSM with ANN and LS-SVM

The capabilities of the proposed LS-SVM, ANN and RSM techniques for the prediction and modeling of the MB adsorption system were evaluated by means of comparing the responses computed from each method to the observed data. For this purpose, the techniques were used to predict the responses belonging to 30 experimental points (the CCD matrix). The performances of the constructed LS-SVM, ANN and RSM models were also statistically measured by R^2 values, RMSE, mean absolute error (MAE) and absolute average deviation (AAD) as follows:

$$R^2 = 1 - \sum_{i=1}^{n} \left(\frac{\left(y_{\text{pred},i} - y_{\text{exp},i}\right)^2}{\left(y_{\text{pred},\,i} - y_{\text{m}}\right)^2} \right) \quad (9)$$

$$\text{RMSE} = \sqrt{\frac{\sum_{i=1}^{n} \left(y_{i,\text{pred}} - y_{i,\text{exp}}\right)^2}{n}} \quad (10)$$

Table 3 Comparison of statistical parameters obtained using the LS-SVM, ANN and RSM models

	Statistical parameters			
Models	R^2	RMSE	AAD%	MAE
LS-SVM	0.9995	0.000229747	0.000600812	0.101417559
ANN	0.9984	0.000989432	−0.033166815	0.145769511
RSM (CCD)	0.9976	0.001233283	−0.003189788	0.157790909

$$\mathrm{MAE} = \frac{\sum_{i=1}^{n} |y_{i,\mathrm{pred}} - y_{i,\mathrm{exp}}|}{n} \quad (11)$$

$$\mathrm{AAD}\% = \left(\frac{1}{n}\sum_{i=1}^{n}\left(\frac{y_{i,\mathrm{pred}} - y_{i,\mathrm{exp}}}{y_{i,\mathrm{pred}}}\right)\right) \times 100 \quad (12)$$

where n is the number of experimental data, $y_{i,\mathrm{pred}}$ and $y_{i,\mathrm{exp}}$ are the predicted and experimental responses, respectively, and $y_{\mathrm{avg,exp}}$ is the average of experimental values.

R^2 measures the percentage of total variation in the response variable that is explained by least-squares regression. R^2 must be closed to 1.0, whereas AAD, which is a direct method for describing deviations between predicted and experimental data, must be as small as possible.

Table 3 presents the statistical comparison (*i.e.* R^2, RMSE, AAD and MAE) of RSM, LS-SVN and ANN models. Generally, all three (RSM, LS-SVM and ANN) models provided good quality predictions in this study; they can be considered to perform well in data fitting and offered stable responses. However, the LS-SVM showed a clear superiority over ANN and RSM. On the other hand, values of the model prediction errors suggest that the RSM prediction performance was relatively poor as compared with the other models applied here. This finding is similar to the usual notion that ANN and SVM regression give better performances than RSM.[46] Residuals *versus* predicted value plots can be more informative regarding model fitting to a data set. If the residuals appear to behave randomly it suggests that the model fits the data well. On the other hand, if a non-random distribution is evident in the residuals, the model does not fit the data adequately. The model-predicted values of the response variable and the residuals corresponding to the experimental data set are plotted in Fig. 5b. The observed

Table 4 Comparison of optimum removal percentage of MB dye from CCD-DF and CCD-GA models

	Models	
Factors	CCD-DF	CCD-GA
pH	7.000	6.999
Adsorbent mass (mg)	0.015	0.015
MB concentration (mg L^{-1})	20.000	20.001
Sonication time (min)	3.000	2.994
$R\%_{\mathrm{MB}}$	98.02	98.125

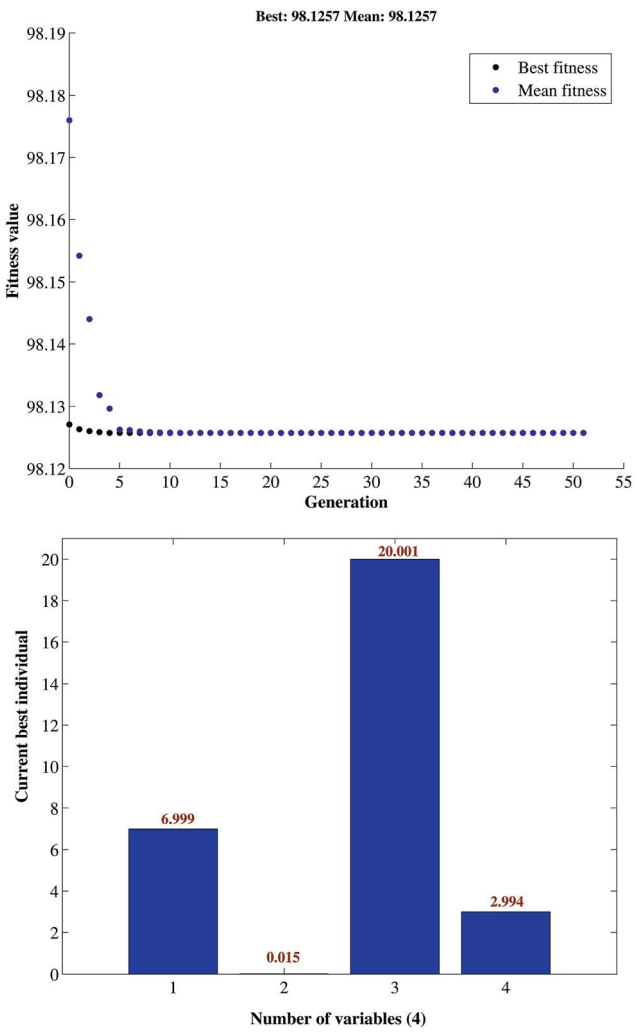

Fig. 6 Plot of fitness value *vs.* generation for the variables in GA optimization of the removal of MB.

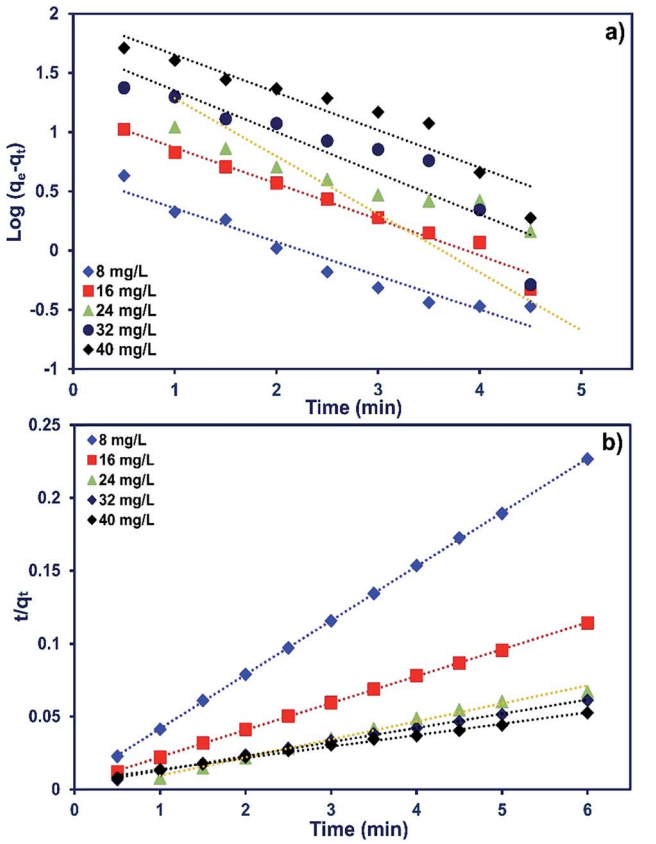

Fig. 7 (a) Pseudo-first-order and (b) second-order kinetic plots for MB adsorption on ZnS-NP-AC (dye concentration: 8–40 mg L^{-1}, adsorbent mass: 0.015 g and pH: 7.0).

relationship between residuals and model-predicted values of removal (R%) yielded by all the three models used here show random distribution and almost complete independence.

The goodness-of-fit between the experimental and the predicted responses given by the LS-SVM, ANN and RSM models are shown in Fig. 5a. The residuals (the differences between predicted and actual values) for both approaches are shown in Fig. 5c which shows the distribution of residuals of the three approaches as a criterion for their compression. The fluctuations of the residuals are relatively small and regular for SVM compared to ANN and RSM. The RSM model shows greater deviation than the LS-SVM and ANN models.

However, there is no vagueness in the RSM model compared with the other approaches, because the RSM model presents all of the relationships between linear, interaction and quadratic effects. Furthermore, the RSM model plays an important role in decreasing the number of experiments, cost and time. In addition, the RSM model optimized the conditions and developed a full quadratic model at optimum conditions.

3.7. Analysis of CCD combined with DF and GA

After performing the experimental design, the response surface and contour plot were drawn using STATISTICA software to guide the determination of optimum values. The optimum values were found to be 7.0, 20 mg L^{-1}, 0.015 g and 3 min for the variables pH, initial MB concentration, adsorbent mass and sonication time, respectively and led to the achievement of a 98.19% removal percentage which was strongly confirmed by five replicates at these conditions that led to a 98.02% ± MB removal percentage.

GA using Matlab R2015a was applied to optimize the input fitness functions formulated in eqn (9) of the CCD for all parameters. According to Table 1, high and low values of each parameter were used to achieve the maximum MB simultaneous removal following the optimization of conditions by GA.

GA optimized values were found to be 6.99, 0.015 g, 20.001 g and 2.994 min for pH, adsorbent mass, MB concentration, and sonication time, respectively. This result was cross-validated by carrying out the batch study at the aforementioned GA-specified optimum conditions. Fig. 6 represents the best fitness plot achieved during the iterations of GA over 50 generations and describes the gradual convergence of results towards the optimal solution.

The optimum conditions for the ultrasound-assisted removal of MB predicted by DF and GA are further compared with experimental results for the same set of parameters (Table 4). This comparison shows a good agreement between the experimental and the predicted data.

3.8. Kinetic studies

The adsorption kinetics of MB onto ZnS-NP-AC were investigated using four kinetic models, namely, the pseudo-first-order,[47] pseudo-second-order,[48] intraparticle diffusion[49] and Elovich[50] models.

The linear plots for pseudo-first-order (Fig. 7a) and pseudo-second-order (Fig. 7b) kinetic models were used to find the

Table 5 Kinetic parameters for MB adsorption onto ZnS-NP-AC

Kinetic model	Plot	Value of parameters						
		Conc. (mg L^{-1})	8	16	24	32	40	
Pseudo-first-order kinetic $\log(q_e - q_t) = \log q_e - \left(\frac{k_1}{2.303}\right)t$	$\ln(q_t - q_e)$ *vs.* t	k_1 (min^{-1})	0.6550	0.6978	1.1280	0.8024	0.7303
		$q_{e(calc)}$ (mg g^{-1})	4.3742	14.856	34.034	50.038	93.239
		R^2	0.9369	0.9770	0.5889	0.8427	0.8975
Pseudo-second-order kinetic $\frac{t}{q_t} = \frac{1}{k_2 q_e^2} + \frac{1}{q_e}t$	t/q_t *vs.* t	k_2 (min^{-1})	0.3059	0.0925	0.0540	0.0281	0.0103
		$q_{e(calc)}$ (mg g^{-1})	26.954	54.054	81.308	103.90	128.21
		R^2	0.9999	0.9998	0.9906	0.9983	0.9951
		h	222.25	270.27	359.99	303.01	169.21
Intraparticle diffusion $q_t = K_{diff}t^{1/2} + C$	q_t *vs.* $t^{1/2}$	K_{diff} (mg g^{-1} min$^{-1/2}$)	2.1578	5.8635	6.1920	14.883	30.944
		C (mg g^{-1})	21.785	39.526	61.084	64.246	44.288
		R^2	0.8260	0.9249	0.9364	0.9737	0.9707
Elovich $q_t = \frac{1}{\beta}\ln(\alpha\beta) + \frac{1}{\beta}\ln t$	q_t *vs.* ln t	β (g mg^{-1})	0.6081	0.2299	0.2197	0.0904	0.0447
		α (mg g^{-1} min^{-1})	72.173	248.30	381.50	935.01	1768.68
		R^2	0.9324	0.9894	0.9831	0.9880	0.9862
Experimental data		$q_{e(exp)}$ (mg g^{-1})	26.421	52.355	74.733	97.381	113.55

Table 6 Adsorption isotherm parameters for MB adsorption onto ZnS-NP-AC

Isotherm	Plot	Parameters	Value of parameters				
			0.005 g	0.010 g	0.015 g	0.020 g	0.025 g
Langmuir $\frac{C_e}{q_e} = \frac{1}{Q_m k_L} + \frac{C_e}{Q_m}$	C_e/q_e *vs.* C_e	Q_m (mg g^{-1})	243.902	161.290	126.584	89.286	73.529
	q_e is the equilibrium MB concentration on adsorbent, Q_m is the maximum amount of adsorption, k_L is the affinity constant, C_e is the solution concentration at equilibrium and R_L is the equilibrium constant it indicates the type of adsorption	k_L (L mg^{-1})	1.323	1.320	4.158	7.467	11.333
		R^2	0.9952	0.9966	0.9934	0.9969	0.9950
		$R_L = (1/(1 + k_L C_0))$	0.0185–0.1313	0.0186–0.1316	0.006–0.0459	0.0033–0.0261	0.0022–0.0173
Freundlich $\ln q_e = \ln K_F + \frac{1}{n} \ln C_e$	$\ln q_e$ *vs.* $\ln C_e$	$1/n$	0.2087	0.3537	0.3446	0.2800	0.2604
	K_F is the Freundlich constant and $1/n$ is the heterogeneity factor describing the adsorption intensity	K_F (L mg^{-1})	8.245	6.763	6.016	6.257	5.990
		R^2	0.9666	0.9646	0.9840	0.8813	0.8861
Temkin $q = B \ln K_T + B \ln C$	q_e *vs.* $\ln C_e$	B	25.172	26.275	18.717	11.979	9.081
	K_T is the equilibrium binding constant corresponding to the maximum binding energy and constant B is related to the heat of adsorption	K_T (L mg^{-1})	469.870	37.072	138.092	368.094	869.55
		R^2	0.8817	0.9803	0.9682	0.9849	0.9832
D-R $\ln q_e = \ln Q_s - \beta\varepsilon^2$	$\ln q_e$ *vs.* ε^2	Q_s (mg g^{-1})	180.187	116.513	91.606	78.007	62.440
	q_e is the amount of adsorbed MB on the adsorbent, Q_s is the maximum adsorption capacity; β is the activity coefficient corresponding to the mean energy of adsorption, E is the free energy and ε is the Polanyi potential	$\beta \times 10^{-8}$	0.796	2.780	1.347	1.280	0.860
		E (kJ mol^{-1})	7.9255	4.2410	6.0926	6.250	7.625
		R^2	0.7083	0.8506	0.8975	0.9629	0.9059

values of their respective parameters. The R^2 values and the various kinetic parameters obtained from the applied kinetic models are shown in Table 5. The values of R^2 for the pseudo-first-order ($\leq$0.9770), intraparticle diffusion ($\leq$0.9737) and Elovich ($\leq$0.9894) kinetic models were low. On the other hand, the values of R^2 for the pseudo-second-order kinetic model were $\geq$0.9983 in most situations and the very reasonable closeness of experimental and predicted q_e values confirmed the high efficiency of this model for representation of the experimental data (Table 5).

3.9. Adsorption isotherms

The equilibrium adsorption isotherms are fundamental in describing the interactive behavior between adsorbates and adsorbent and are essential for giving an idea of the adsorption capacity of the adsorbent. In the present study, four adsorption isotherm models, the Langmuir,[51] Freundlich,[52] Temkin[53] and Dubinin-Radushkevich (D-R)[54] equations, were used to describe the adsorption equilibrium. The Langmuir isotherm is the most popular isotherm model and it is mainly applied to describe monolayer adsorption processes. The Freundlich model is a semi-empirical equation describing heterogeneous surface adsorption and multilayer adsorption under various non-ideal conditions. The Temkin isotherm describes a state in which the heat of adsorption falls linearly with increasing adsorption capacity. D-R is generally applied to express an adsorption mechanism with a Gaussian energy distribution onto a heterogeneous surface.

All adsorption isotherm parameters and R^2 values corresponding to each model are listed in Table 6 based on the respective plots for each model: C_e/q_e *vs.* C_e, $\ln q_e$ *vs.* $\ln C_e$, q_e *vs.* $\ln C_e$ and $\ln q_e$ *vs.* ε^2 straight line plots for the Langmuir, Freundlich, Temkin and D-R models, respectively (Fig. 8a–d).

As can be seen from Table 6, the correlation coefficients and error analysis support the high efficiency of the Langmuir equation ($R^2 \geq 0.9934$) for representing the equilibrium experimental data with a maximum adsorption capacity (Q_m) of 234.90 mg g^{-1}. The R_L values of 0.0022–0.1316 (Table 6) support this high ability and favorability. The less than unity values of $1/n$ point towards a favorable adsorption process. The R^2 values (0.7083–0.9849) for the Freundlich, Temkin and D-R isotherms indicate that these isotherms are not appropriate to describe the experimental data for MB adsorption.

The E value obtained using the D-R constant gives information about adsorption mechanism, physical or chemical. If it lies between 8 and 16 kJ mol^{-1}, the adsorption process takes place chemically, while if $E < 8$ kJ mol^{-1}, the adsorption process proceeds physically. The E values obtained for all adsorbent masses studied in this research were lower than 8 kJ mol^{-1}, which shows that the adsorption of MB onto ZnS-NP-AC occurs by physisorption.

3.10. Performance comparison with other adsorbents

Table 7 compares the sorption capacity (mg g^{-1}), pH and contact time (min) of different nanoparticle adsorbents used

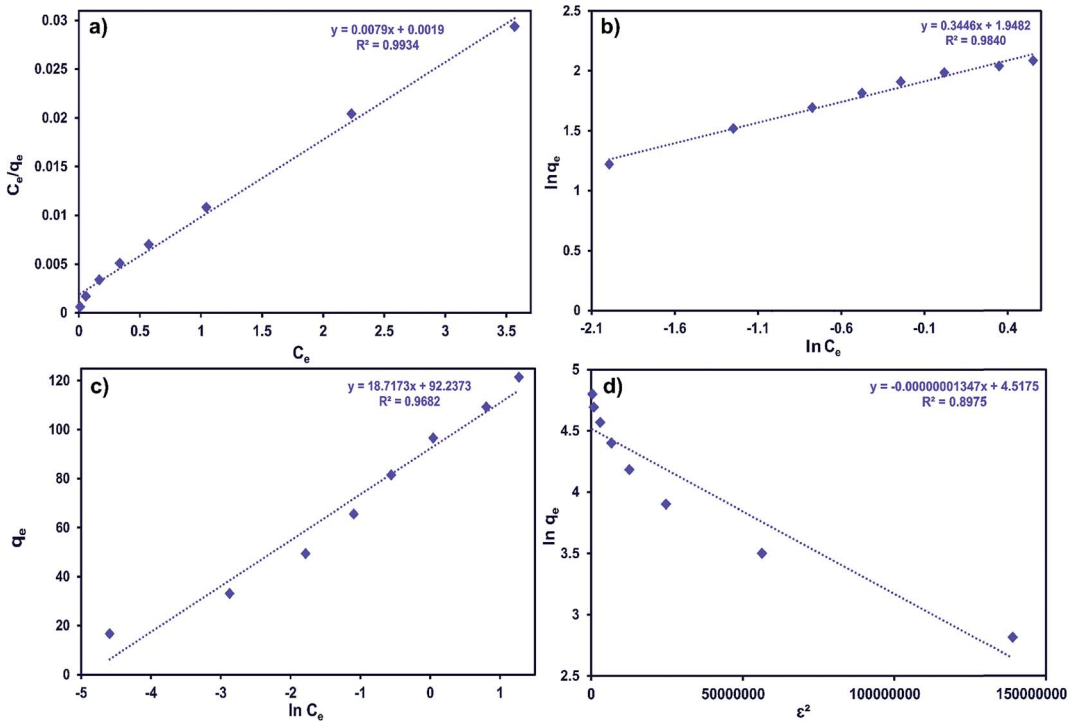

Fig. 8 (a) Langmuir, (b) Freundlich, (c) Temkin and (d) D-R adsorption isotherms for the adsorption of MB onto ZnS-NP-AC (adsorbent mass: 0.015 g, sonication time: 3 min and pH: 7.0).

for the removal of MB. The value of Q_m in this study using an environmentally friendly and low cost adsorbent is significantly higher than those obtained in most of the previous work. As seen in Table 7, the present method is highly recommended due to its higher adsorption capacity over a short time and usage of a small amount of adsorbent, and is favorable for waste water treatment. The present method is preferred and superior to the literature methods in terms of its satisfactory removal performance for dyes as compared to other reported adsorbents.

3.11. Recycling

Regeneration of the adsorbents is important for economic and resource reasons. To assess the adsorption efficiency of the recycled ZnS-NP-AC over nine consecutive cycles, experimental tests were carried out using 50 mL of 20 mg L^{-1} MB solutions, 0.015 g adsorbent and 3 min sonication. Subsequently, the mixture was centrifuged for 3 min at 3000 rpm and the MB adsorption percentage was determined to be 98.20%. The adsorbed MB was efficiently eluted by 10 mL methanol (Fig. 9) and less than 10% in MB removal was seen, while at higher

Table 7 Efficiency of various adsorbents and methods used for MB removal from aqueous solutions

Adsorbent	pH	Sorption capacity (mg g^{-1})	Contact time (min)	Ref.
MWCNTs filled with Fe_2O_3 particles	6.0	42.90	60	55
ZnS : Cu nanoparticles loaded on activated carbon	7.0	106.95	2.2	50
Ag nanoparticles loaded on activated carbon	2.5	71.43	15	14
Au nanoparticles loaded on activated carbon	7.0	185.00	1.6	56
Mn–Fe_3O_4 nanoparticles loaded on activated carbon	5.0	229.40	3.0	44
Fe_3O_4 nanoparticles	6.0	91.90	2.0	57
Oxidized multiwalled carbon nanotubes (MWCNT)	6.0	102.3	2.6	58
Graphene nanosheet/magnetite (Fe_3O_4) composite	6.0	43.83	20	9
NiS nanoparticles loaded on activated carbon	8.1	52.00	5.46	13
CuO nanoparticles loaded on activated carbon	7.0	10.55	15	59
MnO_2 nanoparticles loaded on activated carbon	7.0	234.20	4.0	43
ZnO nanorods loaded on activated carbon	7.0	238.09	20	8
γ-Fe_2O_3-NPs-AC	7.0	195.55	4.0	4
Ru nanoparticles loaded on activated carbon	7.0	185.185	27	60
ZnS nanoparticles loaded on activated carbon	7.0	243.90	3.0	This study

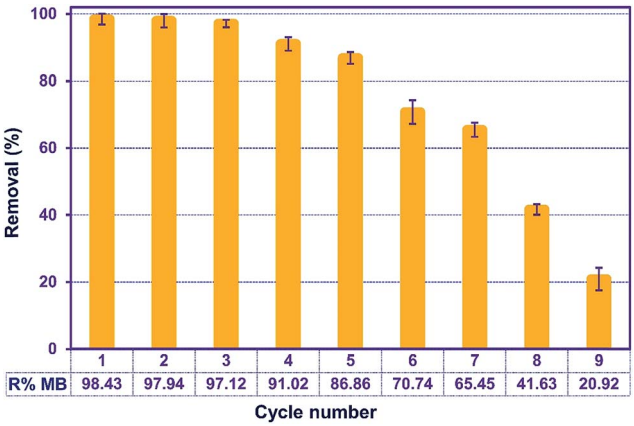

Fig. 9 Effect of the number of regeneration cycles on the adsorption of MB onto ZnS-NP-AC (MB concentration: 20 mg L^{-1}, adsorbent mass: 0.015 g, sonication time: 3 min and pH: 7.0).

times MB molecules strongly attached to the ZnS-NP-AC *via* chemical adsorption.

4. Conclusions

In this study, the main objective was the development and construction of a novel model that could make a reliable prediction of MB adsorption onto ZnS-NPs-AC on the basis of batch adsorption experiments performed with four different process variables (pH, adsorbent mass, MB concentration, and sonication time). LS-SVM, ANN and RSM models were constructed for predicting the removal of MB. Generalization and predictive performances of the different models were evaluated using the statistical criteria of RMSE, R^2, MAE and AAD and analysis of the residuals. All three models predicted the adsorption of MB by ZnS-NPs-AC from aqueous solutions satisfactorily. Based on the findings, the present work indicates that the LS-SVM is much more accurate in modeling the removal of MB dye than the ANN or RSM models. The experimental data from CCD were excellently fitted to the quadratic model, and the relationship between the response and the variables was described by a second-order polynomial equation (regression model). The dosage of ZnS-NPs-AC was the most significant factor for dye removal, followed by pH and sonication time, and the least significant factor was dye concentration. CCD combined with DF and GA methods showed the maximum uptake efficiency for different combinations of pH and MB concentration. The predicted maximum MB adsorption with the corresponding optimal parameters for the adsorption process using DF and GA were as follows: pH 7.00 and 6.99, adsorbent mass 0.015 and 0.015, MB concentration 20.000 and 20.001 mg L^{-1}, and sonication time 3.000 and 2.994 min, respectively. The MB removal process obeys a pseudo-second-order kinetic expression. Adsorption of MB onto the adsorbent follows the Langmuir isotherm. A regeneration study of the material was also carried out and it was found that the ZnS-NP-AC could be regenerated using methanol solution and reused. This report can be used as a stimulus for motivating and inspiring other researchers to develop advanced and optimized systems based on adsorption for the nontoxic and effective treatment of waste water.

Acknowledgements

The authors express their appreciation to the Graduate School and Research Council of the Yasouj University for their financial support.

References

1 L. Cui, X. Guo, Q. Wei, Y. Wang, L. Gao, L. Yan, T. Yan and B. Du, *J. Colloid Interface Sci.*, 2015, **439**, 112–120.
2 V. K. Gupta, R. Jain, T. Saleh, A. Nayak, S. Malathi and S. Agarwal, *Sep. Sci. Technol.*, 2011, **46**, 839–846.
3 S. Dutta, A. Bhattacharyya, A. Ganguly, S. Gupta and S. Basu, *Desalination*, 2011, **275**, 26–36.
4 A. Asfaram, M. Ghaedi, S. Hajati and A. Goudarzi, *Ultrason. Sonochem.*, 2016, **32**, 418–431.
5 M. T. Uddin, M. A. Islam, S. Mahmud and M. Rukanuzzaman, *J. Hazard. Mater.*, 2009, **164**, 53–60.
6 A. Asfaram, M. Ghaedi, S. Hajati, A. Goudarzi and A. A. Bazrafshan, *Spectrochim. Acta, Part A*, 2015, **145**, 203–212.
7 Y. C. Sharma, *J. Chem. Eng. Data*, 2009, **55**, 435–439.
8 M. Ghaedi, A. G. Nasab, S. Khodadoust, R. Sahraei and A. Daneshfar, *J. Ind. Eng. Chem.*, 2015, **21**, 986–993.
9 L. Ai, C. Zhang and Z. Chen, *J. Hazard. Mater.*, 2011, **192**, 1515–1524.
10 F. N. Azad, M. Ghaedi, A. Asfaram, A. Jamshidi, G. Hassani, A. Goudarzi, M. H. A. Azqhandi and A. Ghaedi, *RSC Adv.*, 2016, **6**, 19768–19779.
11 F. Nasiri Azad, M. Ghaedi, K. Dashtian, M. Montazerozohori, S. Hajati and E. Alipanahpour, *RSC Adv.*, 2015, **5**, 61060–61069.
12 S. Hajati, M. Ghaedi and S. Yaghoubi, *J. Ind. Eng. Chem.*, 2015, **21**, 760–767.
13 M. Ghaedi, M. Pakniat, Z. Mahmoudi, S. Hajati, R. Sahraei and A. Daneshfar, *Spectrochim. Acta, Part A*, 2014, **123**, 402–409.
14 M. Ghaedi, S. Heidarpour, S. Nasiri Kokhdan, R. Sahraie, A. Daneshfar and B. Brazesh, *Powder Technol.*, 2012, **228**, 18–25.
15 A. Ahmad, S. H. Mohd-Setapar, C. S. Chuong, A. Khatoon, W. A. Wani, R. Kumar and M. Rafatullah, *RSC Adv.*, 2015, **5**, 30801–30818.
16 S. Agarwal, I. Tyagi, V. K. Gupta, A. R. Bagheri, M. Ghaedi, A. Asfaram, S. Hajati and A. A. Bazrafshan, *J. Environ. Chem. Eng.*, 2016, **4**, 1769–1779.
17 M. K. Sahu, U. K. Sahu and R. K. Patel, *RSC Adv.*, 2015, **5**, 42294–42304.
18 A. Asfaram, M. Ghaedi and G. R. Ghezelbash, *RSC Adv.*, 2016, **6**, 23599–23610.
19 P. Cakir, S. Inan and Y. Altas, *J. Hazard. Mater.*, 2014, **271**, 108–119.

20 G. B. Sahoo, C. Ray, E. Mehnert and D. A. Keefer, *Sci. Total Environ.*, 2006, **367**, 234–251.
21 T. Rajaee, S. A. Mirbagheri, M. Zounemat-Kermani and V. Nourani, *Sci. Total Environ.*, 2009, **407**, 4916–4927.
22 K. Yetilmezsoy and S. Demirel, *J. Hazard. Mater.*, 2008, **153**, 1288–1300.
23 N. G. Turan, B. Mesci and O. Ozgonenel, *Chem. Eng. J.*, 2011, **171**, 1091–1097.
24 R. L. Haupt and S. E. Haupt, *Practical genetic algorithms*, John Wiley & Sons, 2004.
25 S. Kim, K.-S. Sohn and M. Pyo, *ACS Comb. Sci.*, 2011, **13**, 101–106.
26 M. Roosta, M. Ghaedi and A. Asfaram, *RSC Adv.*, 2015, **5**, 57021–57029.
27 A. Asfaram, M. Ghaedi, S. Agarwal, I. Tyagi and V. Kumar Gupta, *RSC Adv.*, 2015, **5**, 18438–18450.
28 M. Ghaedi, H. Z. Khafri, A. Asfaram and A. Goudarzi, *Spectrochim. Acta, Part A*, 2016, **152**, 233–240.
29 M. Ghaedi, E. Alam barakat, A. Asfaram, B. Mirtamizdoust, A. A. Bazrafshan and S. Hajati, *RSC Adv.*, 2015, **5**, 42376–42387.
30 A. R. Bagheri, M. Ghaedi, S. Hajati, A. M. Ghaedi, A. Goudarzi and A. Asfaram, *RSC Adv.*, 2015, **5**, 59335–59343.
31 M. Turabık and B. Gozmen, *Clean: Soil, Air, Water*, 2013, **41**, 1080–1092.
32 V. Vapnik, *The nature of statistical learning theory*, Springer Science & Business Media, 2013.
33 J. A. Suykens, *Eur. J. Contr.*, 2001, **7**, 311–327.
34 K. P. Singh, S. Gupta, P. Ojha and P. Rai, *Environ. Sci. Pollut. Res.*, 2013, **20**, 2271–2287.
35 N. Cristianini and J. Shawe-Taylor, *An introduction to support vector machines and other kernel-based learning methods*, Cambridge university press, 2000.
36 M. Ghaedi, M. Reza Rahimi, A. Ghaedi, I. Tyagi, S. Agarwal and V. K. Gupta, *J. Colloid Interface Sci.*, 2016, **461**, 425–434.
37 E. A. Dil, M. Ghaedi, A. M. Ghaedi, A. Asfaram, A. Goudarzi, S. Hajati, M. Soylak, S. Agarwal and V. K. Gupta, *J. Ind. Eng. Chem.*, 2016, **34**, 186–197.
38 A. Bouchachia, *Adaptive and Intelligent Systems: Third International Conference, ICAIS 2014, Bournemouth, UK, September 8-9, 2014, Proceedings*, Springer, 2014.
39 A. Khataee and M. Kasiri, *J. Mol. Catal. A: Chem.*, 2010, **331**, 86–100.
40 F. Nasiri Azad, M. Ghaedi, K. Dashtian, M. Montazerozohori, S. Hajati and E. Alipanahpour, *RSC Adv.*, 2015, **5**, 61060–61069.
41 M. Kuppayee, G. K. Vanathi Nachiyar and V. Ramasamy, *Appl. Surf. Sci.*, 2011, **257**, 6779–6786.
42 I. Parvaneh, S. Samira and N. Mohsen, *Chin. Phys. B*, 2015, **24**, 46–50.
43 A. Asfaram, M. Ghaedi, S. Hajati and A. Goudarzi, *RSC Adv.*, 2015, **5**, 72300–72320.
44 A. Asfaram, M. Ghaedi, A. Goudarzi and M. Rajabi, *Dalton Trans.*, 2015, **44**, 14707–14723.
45 M. Ghaedi, Z. Rozkhoosh, A. Asfaram, B. Mirtamizdoust, Z. Mahmoudi and A. A. Bazrafshan, *Spectrochim. Acta, Part A*, 2015, **138**, 176–186.
46 M. Jamshidi, M. Ghaedi, K. Dashtian, A. M. Ghaedi, S. Hajati, A. Goudarzi and E. Alipanahpour, *Spectrochim. Acta, Part A*, 2016, **153**, 257–267.
47 Y. Tang, T. Hu, Y. Zeng, Q. Zhou and Y. Peng, *RSC Adv.*, 2015, **5**, 3757–3766.
48 T. G. Yan and L. J. Wang, *Water Sci. Technol.*, 2014, **69**, 612–621.
49 Z. Ioannou and J. Simitzis, *Water Sci. Technol.*, 2013, **67**, 1688–1694.
50 A. Asfaram, M. Ghaedi, S. Hajati, M. Rezaeinejad, A. Goudarzi and M. K. Purkait, *J. Taiwan Inst. Chem. Eng.*, 2015, **53**, 80–91.
51 J. Fu, Z. Chen, M. Wang, S. Liu, J. Zhang, J. Zhang, R. Han and Q. Xu, *Chem. Eng. J.*, 2015, **259**, 53–61.
52 J. J. Gao, Y. B. Qin, T. Zhou, D. D. Cao, P. Xu, D. Hochstetter and Y. F. Wang, *J. Zhejiang Univ., Sci., B*, 2013, **14**, 650–658.
53 L. Ai, C. Zhang, F. Liao, Y. Wang, M. Li, L. Meng and J. Jiang, *J. Hazard. Mater.*, 2011, **198**, 282–290.
54 F. N. Azad, M. Ghaedi, K. Dashtian, S. Hajati and V. Pezeshkpour, *Ultrason. Sonochem.*, 2016, **31**, 383–393.
55 S. Qu, F. Huang, S. Yu, G. Chen and J. Kong, *J. Hazard. Mater.*, 2008, **160**, 643–647.
56 M. Roosta, M. Ghaedi, A. Daneshfar, R. Sahraei and A. Asghari, *Ultrason. Sonochem.*, 2014, **21**, 242–252.
57 M. Ghaedi, S. Hajjati, Z. Mahmudi, I. Tyagi, S. Agarwal, A. Maity and V. Gupta, *Chem. Eng. J.*, 2015, **268**, 28–37.
58 M. Ghaedi, S. Hajati, M. Zare, M. Zare and S. Y. Shajaripour Jaberi, *RSC Adv.*, 2015, **5**, 38939–38947.
59 M. Ghaedi, A. Ghaedi, M. Hossainpour, A. Ansari, M. Habibi and A. Asghari, *J. Ind. Eng. Chem.*, 2014, **20**, 1641–1649.
60 H. Mazaheri, M. Ghaedi, S. Hajati, K. Dashtian and M. K. Purkait, *RSC Adv.*, 2015, **5**, 83427–83435.